CHARACTERISATION OF ELECTRO-OPTIC PICKUPS FOR HIGH BANDWIDTH DIAGNOSTICS AT THE HIGH LUMINOSITY LHC

A. Arteche*, S. E. Bashforth, A. Bosco, S. M. Gibson, I. Penman
JAI at Royal Holloway, University of London, Egham, UK
M.Krupa, T. Lefèvre, CERN, Geneva, Swizerland

Abstract

A high bandwidth electro-optical beam position monitor is under development for the High Luminosity LHC. A series of measurements of the electro-optic signals were previously obtained by an EO-BPM prototype installed in the SPS. This paper focuses on an advanced design that would further improve the sensitivity of the pick-up by optimising the shape of the metallic electrode mounted onto the crystal. The proposed upgraded electro-optic pickups significantly increase the image field profile of the passing bunch inside a lithium niobate crystal embedded within the pickup. This work is based on parametric studies, performed using CST particle studio, investigating various electro-optic (electrode and crystal) configurations. We present the expected performance of the different designs, alongside with their evaluation on a test bench, highlighting the most relevant choice for a prototype pick-up to be installed on LHC.

INTRODUCTION

The EO-BPM technology has been proposed as a diagnostic tool to monitor the bunch crabbing and detect high order intra-bunch perturbations at the future High-Luminosity LHC [1, 2]. The fast optical response induced by the ultra-relativistic Coulomb field is designed to follow the transverse position along $4\sigma \sim 1$ ns for the nominal HL-LHC bunch length of 1.15×10^{11} protons, with an operational bandwidth between 6 GHz – 12 GHz.

The performance of the EO-BPM relies on the Electro-Optic (EO) interaction of the Lithium Niobate (LNB) crystal assembled between electrodes in the core of each Pick-Up (PU) and the beam-induced modulating field E_{LNB}. The crystal birefringence is modified with the passing beam, producing a phase retardation subject to be delivered in form of optical modulation into fast detectors.

Upgrade Target

Previous PU variant one (PU-one) proved that the floating electrode facing the beam can direct an amplified image field strength E_{LNB} of the Coulomb field E_{Coulomb} into the crystal [3]:

$$E_{\text{LNB}} = \mu_C \frac{E_{\text{Coulomb}}(r_0)}{\epsilon_r},\tag{1}$$

where μ_C is the amplifying coupling factor, r_0 the radial position of the crystal, and $\epsilon_r = 30$ is the relative dielectric constant of LNB. This approach aimed to overcome the

_____
* alberto.arteche@rhul.ac.uk

field reduction caused by ϵ_r in Eq. (1) and was validated by the overall increase factor ~ 8 measured in the SPS in 2017 [4, 5]. Particularly, the EO PU prototype installed in the SPS detected modulations below 1% of the transfer function range for PU-one at Crossed Polarisers (CP) caused by small modulating fields (< 3 kV/m) with respect to its characteristic E_π parameter (~ 400 kV/m) [5].

The upgrade strategy consists essentially of maximizing the ratio E_{LNB}/E_π. The reliability of the Single Crystal Interferometric (SCI) arrangement that offers a 1.45 reduction factor in E_π was successfully tested in 2017 in the SPS [6]. Based on those results, an extra factor two given by the Double Crystal Interferometric (DCI) is considered. In addition, the optimization of the floating electrode shown later on targets to enhance E_{LNB} up to a range between $30 - 50$ kV/m, that is, at least 10 times higher than PU-one in the SPS.

Figure 1 shows the transfer functions that determine the EO performance for the three configurations considered, assuming a 9 mm long crystal working at $\lambda = 780$ nm to avoid photorefractivity in LNB, and a natural birefringence offset such that the signal scales up along the linear response region. Above 30 kV/m at DCI, the optical modulation is more than 30 times better than for PU-one at CP, increasing the signal from 1 % to a significant portion of the transfer function (~ 30%); however, it should be noticed that beyond $50-60$ kV/m at DCI the system gradually looses the linearity which implies the EO upgrade limit is reached. Further improvements may concern the acquisition system, which is independent of the EO optimisation discussed in this paper.
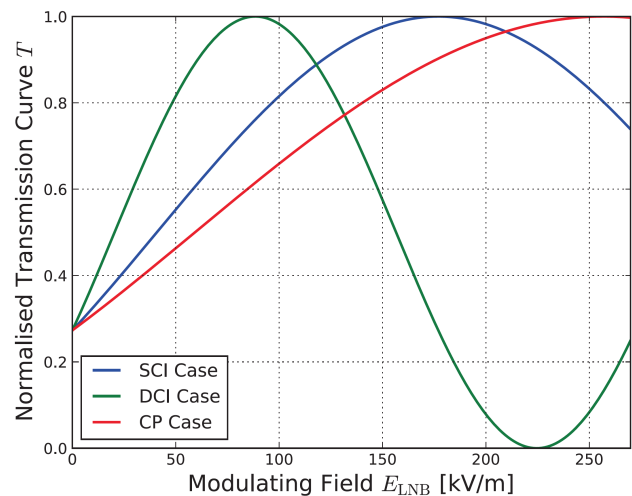

Figure 1: Transfer functions for a 9 mm long LNB crystal at 780 nm for the three main EO configurations considered.

MC6: Beam Instrumentation, Controls, Feedback and Operational Aspects

T03 Beam Diagnostics and Instrumentation

ELECTRO-MAGNETIC SIMULATIONS

Simulation studies on the floating electrode geometry have been conducted to maximize E_{LNB} within the target range set up in the preceding section. Previous results indicate that T-shaped and rod-shaped electrodes must not be used in order to avoid auto-inductance effects and subsequent field resonances [3]. Due to this reason, a floating pyramidal design has been proposed and the top electrode is now totally flat against the LNB crystal.

The electro-magnetic numeric results shown in this paper have been obtained with CST particle studio [7]. Figure 2 shows the front view section of the PU design in the CST interface: whereas the top electrode is grounded, the copper floating electrode on the bottom is only in contact with a macor ceramic support that works as an electric insulator. Then the Coulomb field E_{Coulomb} propagating from the proton beam traveling along y is collected at the outer face of the electrode, and delivered more concentrated into the LNB sample that also accounts for the dielectric constant ϵ_r decay. In future, the upgraded PU model may incorporate a controlled discharge mechanism for the floating electrode.

The simulations now consider the LHC parameters, including a pipe radius $r_0 = 44.5\,\text{mm}$, which makes the PU closer to the beam by 22 mm with respect to the SPS case ($r_0 = 66.5\,\text{mm}$). It can be observed that the macor support has also been simplified to reduce possible resonating cavities and improve the impedance.
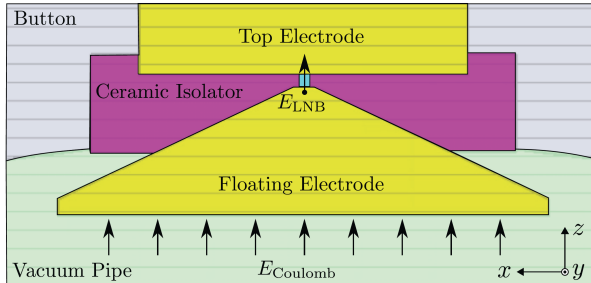

Figure 2: Front view section.

Figure 3 shows the longitudinal side view section of the upgraded PU: the Optical Beam (OB) path is shown along through the crystal parallel to y and the proton beam direction. The crystal length L_y is fixed to 9 mm to prevent potential bandwidth limitations, however, the electrode profile has also been made pyramidal on the zx plane to increase the collected field. It should be noticed that due to phase-matching considerations, the y dimension of the floating electrode can potentially be increased up to $n_z \times L_y \sim 20\,\text{mm}$, where n_z is the LNB refractive index on the optical polarisation direction.

Figure 4 shows how the xz-plane of the crystal has significantly been reduced to favour the field concentration along the LNB crystallographic direction z, making the input optical face a $0.3\,\text{mm}^2$ square section.

Mathematically, the overall field-collecting performance of the PU is characterized by the gain factor μ_C shown
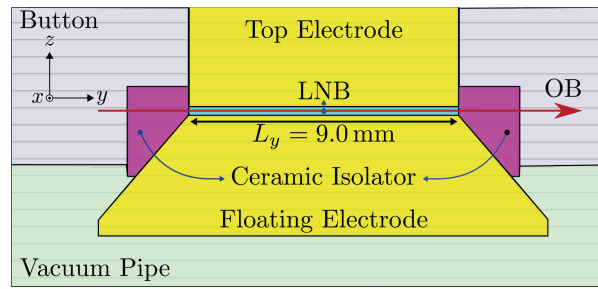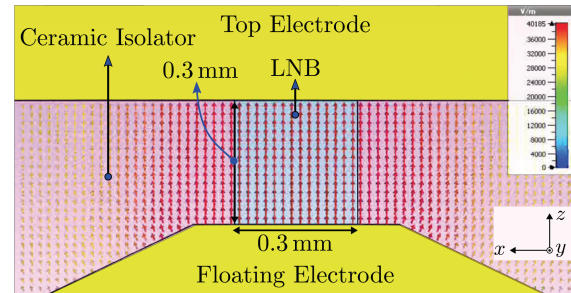

Figure 3: Side view section.

Figure 4: 0.3×0.3 zoomed-in front section along with the field simulation.

in Eq. (1). With this proposal, $\mu_C \simeq 34$, which implies a significant increment with respect to PU-one ($\mu_C \simeq 3$). Figure 5 shows a comparison between the E_{LNB} time-profile in both cases: it can be observed an increment from below $3\,\text{kV/m}$ for PU one to more than $40\,\text{kV/m}$, thus the field target established in the preceding section is met by this design, according to the CST output.
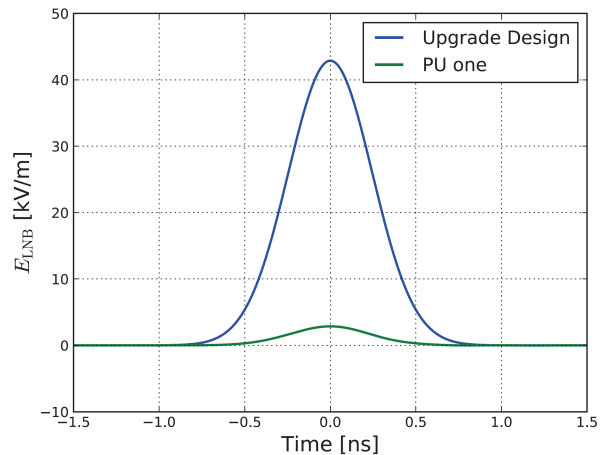

Figure 5: Modulating field comparison between PU one and the upgrade design.

EXPERIMENTAL TEST OF THE DCI CONFIGURATION

In addition to the field increment provided by the design upgrade, a DCI approach is studied to improve the sensitivity by a factor ~ 3. The optical bench setup shown in Fig. 6 has been developed to test this configuration: a collimated

MC6: Beam Instrumentation, Controls, Feedback and Operational Aspects

T03 Beam Diagnostics and Instrumentation

780 nm OB is made pass through a EO PU-one that was adapted to hold 2 LNB 9 mm long crystals disposed as shown in Fig. 7 inside the button. The OB is linearly polarised along the z-direction of the crystals, which are inversely poled thus each of them produces a phase retardation of different sign, doubling the effect. The optical path is aligned to ensure the incoming OB is evenly distributed on both optical faces so after the PU the beam splits into two spots that are inversely modulated when E_{LNB} is applied. The beam is then focused using a $f = 800$ mm lens to make both sections interfere along a large Rayleigh length distance and coupled back into a 100 μm multimode fiber.
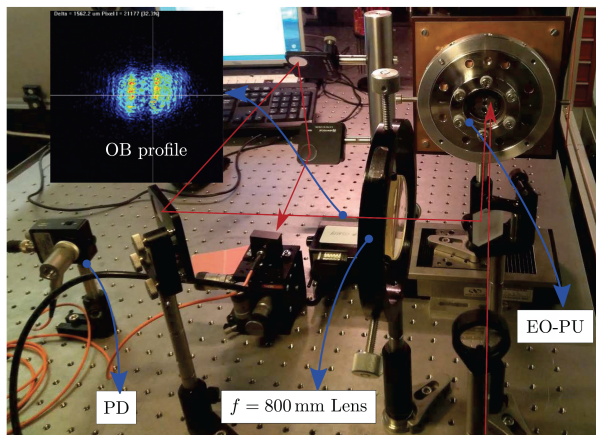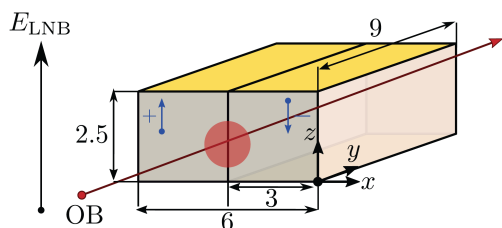

Figure 6: Test bench setup.

Figure 7: DCI configuration setup inside the modified PU-one.

The PU is held by a steel ring and the full output V from a sinusoidal voltage source was connected to an in-house designed plate clamped to the electrode of the EO button on the back side of the flange. Figure 9 shows the typical modulation fringes captured by a Photodetector (PD) while a modulating field $E_{LNB} = V/L_y$ was applied by the generator at different voltage amplitudes. Note that arbitrary baseline offsets have been introduced to separate the AC traces acquired. The optical response follows the input signal correctly and it is clearly detectable at 4 kV/m, which is slightly above PU-one coupling performance. As expected, Fig. 8 proves that the modulation is in fact proportional to the field applied.

CONCLUSION

Forthcoming improvements of the EO performance comprise two main strategies: a factor 10 enhancement of the
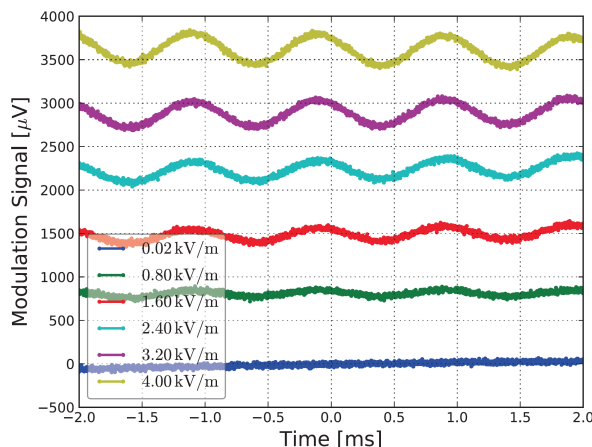

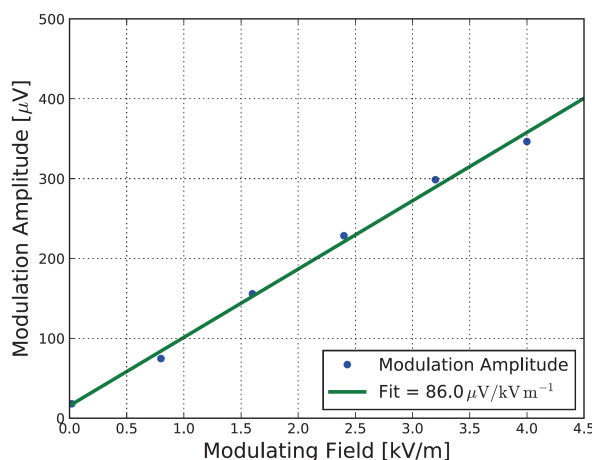Figure 8: Modulation fringes at different modulating field strengths.

Figure 9: Modulation amplitude against modulating field strength.

modulating field by optimising the floating electrode and the overall PU; the employment of the 3 times more sensitive DCI configuration. Therefore, the overall upgrade is expected to be above a factor 30, pushing the system efficiency towards a working point that covers most of the linear response region of the transfer function.

ACKNOWLEDGEMENTS

REFERENCES

[1] G. Apollinari *et al.*, "High-Luminosity Large Hadron Collider (HL-LHC): Technical Design Report V. 0.1", CERN-2017-007-M, Yellow Report., 2017. doi:10.23731/CYRM-2017-004

[2] S. Gibson *et al.*, "High Frequency Electro-Optic Beam Position Monitors for Intra-Bunch Diagnostics at the LHC",in *Proc. IBIC'15*, Melbourne, Australia, Sep. 2015, pp. 606–610. doi:10.18429/JACoW-IBIC2015-WEDLA02

[3] A. Arteche, Studies of a prototype of an Electro-Optic Beam Position Monitor at the CERN Super Proton Synchrotron, Ph.D. Thesis, Royal Holloway, University of London, 2018.

[4] A. Arteche *et al.*, "Development of a Prototype Electro-Optic Beam Position Monitor at the CERN SPS", in *Proc. IBIC'16*, Barcelona, Spain, Sep. 2016, pp. 634–637. `doi:10.18429/JACoW-IBIC2016-WEPG09`

[5] A. Arteche *et al.*, "First Beam Tests at the CERN SPS of an Electro-Optic Beam Position Monitor for the HL-LHC", in *Proc. IBIC'17*, Grand Rapids, MI, USA, Aug. 2017, pp. 270–273. `doi:10.18429/JACoW-IBIC2017-TUPCF23`

[6] S. Gibson *et al.*, "Enhanced Bunch Monitoring by Interferometric Electro-Optic Methods", in *Proc. IPAC'18*, Vancouver, Canada, Apr.-May 2018, pp. 2353–2356. `doi:10.18429/JACoW-IPAC2018-WEPAL073`

[7] Computer Simulation Technology, `https://www.cst.com/`